



Multifunctional carbon fiber@NiCo/polyimide films with outstanding electromagnetic interference shielding performance

Jianwei Li^{a,*}, Xuanning Zhang^a, Yuanqing Ding^a, Shengyao Zhao^c, Zhonglei Ma^{b,*}, Hongming Zhang^b, Xinhai He^a

^a School of Materials Science and Engineering, Xi'an Polytechnic University, Xi'an 710048, China

^b Shaanxi Key Laboratory of Macromolecular Science and Technology, School of Chemical and Chemical Engineering, Northwestern Polytechnical University, Xi'an 710072, China

^c School of Materials Science and Engineering, Shandong University, Jinan 250100, China



ARTICLE INFO

Keywords:

Carbon fiber
NiCo₂O₄ nanowires
NiCo alloy
EMI shielding
Thermal management

ABSTRACT

The electromagnetic interference (EMI) shielding materials with low reflection characteristics are highly desirable for integrated communication and microelectronics systems to shield EM waves and their secondary pollution. In this study, the EMI shielding materials with outstanding absorption performance were fabricated via the two-step pyrolysis and followed by vacuum assisted filtration approach. The chopped carbon fibers (CFs) wrapped with NiCo₂O₄ nanowire arrays (CF@NiCo₂O₄) were prepared by the hydrothermal reaction initially. After annealing, the NiCo₂O₄ nanowires transformed into NiCo alloy nanoparticles and evenly embedded in the CFs, endowing the CF@NiCo composites with efficient magnetic loss and dielectric loss capacity. After vacuum filtration and encapsulation with polyimide, the obtained flexible CF@NiCo/polyimide composite film displays superior EMI shielding effectiveness of 87 dB with a thickness of only 1.08 mm. Particularly, the composite film exhibits extremely low SE_R characteristics of ~6 dB, which surpasses those of most previously reported composites materials with similar thickness. In addition, the composite films present outstanding flexibility, mechanical properties and Joule heating performances. Therefore, the prepared flexible composite films have broad prospect for EMI shielding and thermal management applications in advanced microelectronic systems.

1. Introduction

With the increasing popularity of flexible electronics, integrated microelectronics and wireless 5G telecommunication devices, higher requirements are imposed on the electromagnetic interface (EMI) shielding materials to ensure the safety of microelectronic system [1–3]. Especially, the EMI shielding materials with the ultra-low reflection characteristics are urgently desired to prevent the secondary wave pollution. To date, various EMI shielding materials with excellent shielding performance have been fabricated based on the mechanisms of the reflection, absorption, and multiple reflections of the EM waves [4,5]. However, the reflection is still the dominated mechanism in these studies. EM wave transmission theory indicate that the impedance matching is a critical factor to design the absorption dominated EMI shielding materials [6]. Up to present, although abundant efforts have been devoted to this topic, the exploration of EM shielding materials with low reflection characteristics that could satisfy practical

application still remains challenge.

According to the EMI shielding mechanisms, the electrical conductivity is the basic principle for the design of EMI shielding materials as the charge carriers can interact with the incident EM waves [7–9]. However, the single high electrical conductivity will bring poor absorption characteristics due to the impedance mismatching [10,11]. Therefore, a large proportion of incident EM waves are inevitably reflected, thus the multiple EM attenuation mechanisms should be introduced to design the high-absorption dominated EMI shielding materials, such as internal multiple reflection, dielectric loss, electromagnetic dipoles, magnetic loss and etc. Especially, the introduction of auxiliary magnetic component has aroused wide concerns, as the magnetic component could balance the electric-magnetic properties of the EMI shielding materials. The elevated impedance matching enables the EM waves to enter the EMI shielding materials as many as possible instead of reflection [12–14]. Moreover, the incident EM waves could be further attenuated by the multiple loss effects, resulting in the improvement in

* Corresponding authors.

E-mail addresses: lijianwei@xpu.edu.cn (J. Li), mazl@nwpu.edu.cn (Z. Ma).

the absorption portion of the incident EM waves.

Based on the theory mentioned above, many efforts have been devoted to develop wave-absorption dominated EMI shielding materials containing electronic/magnetic components, [15–17] including the polymer-based composites, ceramic-based composites and carbon-based composites [18–21]. Especially, the polymer-based composites possess the attractive advantages of shaping capability, chemical stability and design flexibility. The corresponding structural design strategies mainly include electroless plating and electromagnetic component filling [22–26]. Electroless plating is an effective method to fabricate the EMI shielding materials with tunable electromagnetic parameters [27,28]. The hydrazine hydrate, sodium borohydride solution, sodium hypophosphite etc. have been usually used to reduce the Fe^{2+} , Co^{2+} and Ni^{2+} into zero-valence Fe, Co, Ni and further deposited on the surface of the polymer substrate [29]. By controlling the composition and relative content of the electric/magnetic components, the dielectric-magnetic characteristics of the composites were balanced and the absorption dominated EMI shielding performance could be obtained. Recently, various substrates have been selected to fabricate this kind of composites with magnetic metal or alloy plating, such as the polyimide nanofibrous films, polypropylene fabrics, poly(vinylidene fluoride) based films, polymer foams and etc [30,31]. However, how to ensure the stable bonding between the plating and substrate is still an obstacle for practical application of this kind of materials.

An alternative method is to introduce the magnetic or electronic/magnetic fillers into the polymer or conductive polymer matrix [32,33]. Through regulating the relative contents of conductive and magnetic components, the dielectric constant and permeability of the composite materials could be balanced, so as to achieve the desirable impedance matching and electromagnetic loss [34–36]. Duan et al. designed an asymmetric polyurethane composite foam with a unique asymmetric Ag-coated conductive network and oriented porous structure, the graphene-supported iron-cobalt (FeCo@rGO) magnetic nanoparticles were chosen as the electrical and magnetic functional components to regulate the impedance matching. The composite foam exhibits an outstanding EMI shielding efficiency of 84.8 dB with the thickness of 0.4 cm, while the reflection efficiency is only 0.3 dB [37]. However, the limitation associated with this method is the aggregation of the functional nanofillers, which determines the upper limit of the EMI shielding performance and is unfavorable for the mechanical properties of the materials.

At present, the EMI shielding materials with the characteristics of “lightweight, ultrathin, flexible and high-performance” are greatly desirable to meet practical applications in the high-end manufacturing industries such as aviation, aerospace, microelectronics, portable telecommunication and etc [38]. For example, most parts of devices have special shapes and work at the complex environments. Therefore, the EMI shielding materials should be able to withstand harsh environments and exhibit certain flexibility for various practical applications. However, up to date, it still remains a challenge to fabricate the absorption dominant EMI shielding materials with the combined characteristics of “lightweight, ultrathin, flexible and high-performance”.

In this work, we aim to design and fabricate the flexible and mechanically strong EMI shielding composite films with low reflection characteristics. Specifically, the chopped CFs were chosen as the substrate to construct the conductive networks, and the magnetic metal nanoparticles decorated on the CF ($\text{CF@magnetic metals}$) through hydrothermal reaction and carbothermic reaction were designed as the EM wave absorption nanofillers. Afterwards, the flexible EMI shielding films were prepared via vacuum-assistant filtration and encapsulated with polyimide (PI). The special engineering polymer PI could endow the composite films with advantages of excellent mechanical properties, chemical resistance and thermal stability. The synergistic effect derived from the magnetic metal nanoparticles and conductive CFs endows the flexible films with balanced electric-magnetic properties, and thus enhancing the absorption and attenuation efficiency of the EM waves.

The morphologies and chemical structures of the composites were systematically characterized. The EM shielding performance and the practical application properties including mechanical properties and flexibility were also investigated in detail.

2. Experimental

2.1. Materials

The $\text{Ni}(\text{NO}_3)_2 \cdot 6\text{H}_2\text{O}$ and $\text{Co}(\text{NO}_3)_2 \cdot 6\text{H}_2\text{O}$ were supplied by Heowns Co. Ltd. (Tianjin, China). 3,3',4,4'-benzophenonetetracarboxylic dianhydride (BTDA) and 4,4'-diaminodiphenyl ether (ODA) were purchased from Aladdin Industrial Co., Ltd. (Shanghai, China). Anhydrous ethanol $\text{CO}(\text{NH}_2)_2$, N,N-dimethylformamide and nitric acid were purchased from Tianjin FuYu Chemical Co., Ltd. (Tianjin, China). The chopped carbon fibers (CFs) with the length of 100 ~ 1000 μm were provided by Liso composite materials Co., Ltd. All reagents were analytically grade and used as received. The deionized (DI) water was obtained in the laboratory.

2.2. Preparation of CF@NiCo composites

The chopped CFs decorated with NiCo_2O_4 nanowire arrays ($\text{CF@NiCo}_2\text{O}_4$) were fabricated initially. 0.29 g of $\text{Ni}(\text{NO}_3)_2 \cdot 6\text{H}_2\text{O}$, 0.58 g of $\text{Co}(\text{NO}_3)_2 \cdot 6\text{H}_2\text{O}$ and 0.72 g of $\text{CO}(\text{NH}_2)_2$ were dissolved in 70 mL deionized water by stirring and then transferred into a 100 mL Teflon-lined stainless autoclave. Besides, 0.5 g of chopped CFs were etched in nitric acid for 12 h, washed with deionized water for several times, then immersed in the above solution and dispersed ultrasonically for 30 min. The sealed autoclave was treated at 120 °C for 8 h. After the reaction, the resulting products were collected and rinsed with deionized water and then heated at 400 °C for 2 h under the N_2 atmosphere to obtain the NiCo_2O_4 nanowire arrays. Afterwards, the prepared $\text{CF@NiCo}_2\text{O}_4$ composites were placed in a tube furnace and further treated at 800 °C for 2 h under the N_2 atmosphere, thus the CF@NiCo composites were obtained by the carbothermic reaction.

2.3. Preparation of CF@NiCo/PI films

The prepared CF@NiCo composites were ultrasonically dispersed in the water and a buchner funnel with a diameter of 7 cm was used for filtration. The fabricated composite CF@NiCo fabrics were peeled off from the filter paper and further dried at 60 °C for 5 h, then the polyamic acid (PAA)/DMAc solution pre-synthesized by the BTDA and ODA with the solid content of 10 wt% was evenly dropped on the CF@NiCo fabrics until the PAA solution was saturated. Finally, a series of CF@NiCo/PI films were fabricated respectively after hot-pressing and curing at 260 °C for 2 h. In these cases, the thickness of composite films can be adjusted by adding different amounts of CF@NiCo composites for filtration. For comparison, a series of pure CF/PI and $\text{CF@NiCo}_2\text{O}_4/\text{PI}$ films with different amounts of CFs and $\text{CF@NiCo}_2\text{O}_4$ were also prepared via the same method. Specifically, the amounts of the CFs, $\text{CF@NiCo}_2\text{O}_4$ and CF@NiCo added into the dispersion for filtration were 0.2 g, 0.4 g, 0.6 g, 0.8 g and 1.0 g, respectively. The corresponding films were denoted as CF/PI-X , $\text{CF@NiCo}_2\text{O}_4/\text{PI-X}$ and CF@NiCo/PI-X correspondingly, where the X are 0.2, 0.4, 0.6, 0.8 and 1.0, respectively. The specific fabrication processes of CF@NiCo and CF@NiCo/PI films are illustrated in the Fig. 1.

2.4. Characterization

The morphologies and element distribution of the samples were characterized by VEGA 3 scanning electron microscope (TESCAN, Czech Republic) with an energy dispersive X-ray spectroscopy (EDX) elemental mapping. The chemical structures of the samples were measured by XRD, Raman and X-ray photoelectron spectra (XPS). Specifically, the

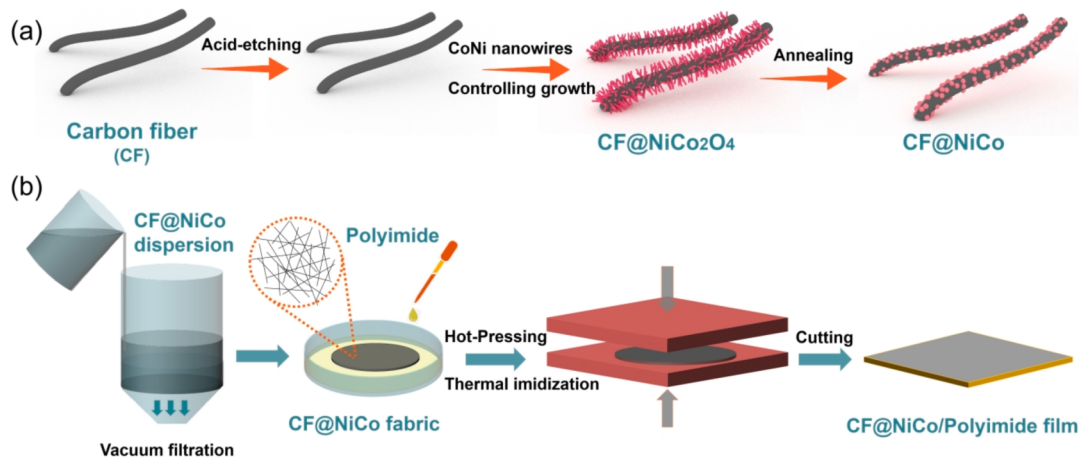


Fig. 1. (a) Schematic illustration of the synthesis process of CF@NiCo composites. (b) Fabrication procedure of the CF@NiCo/PI films.

XPS spectra measurements were performed by X-ray photoelectron spectroscopy (Kratos Axis Ultra DLD, Britain) with scanning monochromatic Al-K α X-ray source (1486.6 eV). The powder X-ray diffraction (XRD) studies were carried out in the range of $2\theta = 5^\circ$ – 80° with a scanning rate of 8° min^{-1} . Raman spectra were recorded by WITec Alpha-300R Raman spectroscopy system. The magnetic properties of CF@NiCo composites were measured at 300 K with a Lake Shore 7410 vibrating sample magnetometer (VSM). The conductivities of the samples were tested using a Rooko four-probe tester (FT-334, China). The mechanical properties of the composite films were tested using the CMT 8502 multifunctional experimental machine (SANS, Shenzhen, China). The relatively complex permittivity ($\epsilon_r = \epsilon' - j\epsilon''$) and permeability ($\mu_r = \mu' - j\mu''$) were determined in the frequency range of 2–18 GHz. The samples were homogeneously dispersed in paraffin according to the sample-to-paraffin mass ratio of 4:6 and pressed into a toroidal shape with an inner diameter of 3.04 mm and outer diameter of 7.0 mm. The EMI shielding performances of composite films were measured using the waveguide method by an Agilent PAN-N5232A vector network analyzer in the frequency range of 8.2–12.4 GHz (X-band). The scattering parameters of S11 (input reflection) and S21 (reverse transmission) in the frequency range of 8.2–12.4 GHz were recorded to calculate the reflection coefficient (R), transmission coefficient (T) and absorption coefficient (A), the contributions of the microwave reflection (SE_R) and microwave absorption (SE_A) to the total EMI shielding efficiency (SE_T) were calculated using the following equations:

$$SE_{\text{Total}}(\text{dB}) = 10\lg\left(\frac{P_I}{P_T}\right) = SE_R + SE_A + SE_M \quad (1)$$

$$T = |S_{21}|^2, R = |S_{11}|^2, A = 1 - T - R \quad (2)$$

$$SE_A = 10\lg\left(\frac{1 - |S_{11}|^2}{|S_{21}|^2}\right) \quad (3)$$

$$SE_R = 10\lg\left(\frac{1}{1 - |S_{11}|^2}\right) \quad (4)$$

Moreover, to compare the effectiveness of shielding materials, the specific shielding effectiveness (SSE) and SSE/t taking the density and thickness into account are represented as follows:

$$SSE = \text{EMI SE}/\text{density} = \text{dB} \cdot \text{cm}^3 \cdot \text{g}^{-1} \quad (5)$$

$$SSE/t = \text{SSE}/\text{thickness} = \text{dB} \cdot \text{cm}^2 \cdot \text{g}^{-1} \quad (6)$$

3. Results and discussion

3.1. Fabrication and morphologies of CF@NiCo composites

The NiCo alloy nanoparticles decorated on the chopped carbon fibers (CF@NiCo) were fabricated by a hydrothermal reaction, followed by heat treatment at 800 °C in N₂ atmosphere. The CF@NiCo with different nanoparticle loading can be adjusted by regulating the relative amount of the CFs and metal salts (with constant molar ratio of 1:2 for Ni²⁺: Co²⁺). The morphologies and structures of pristine CFs and prepared magnetic CF composites that carbonized at 400 °C and 800 °C were characterized by the SEM. Fig. 2a shows that the pure CFs possess the smooth surface and their average diameter is about 9 μm. After the acid etching treatment and hydrothermal reaction, the needle like NiCo₂O₄ nanowires are completely coated the CFs, and the original morphology of CFs could not be observed (Fig. 2 b, c). The mass loading of NiCo₂O₄ on the CF was measured to be around 26 mg/g, indicating that the relative content of the NiCo₂O₄ nanowires in CF@NiCo₂O₄ is about 2.0–3.0 wt%. Moreover, the experiment indicates that the acid etching treatment has great influence on the growth of NiCo₂O₄ nanowires on the CF surfaces. Without the etching treatment, only part of surface was covered by uneven NiCo₂O₄ nanowires after hydrothermal reaction, and the agglomeration occurred generally. It is mainly caused by the sizing agent coated on the fiber surfaces that should be removed by acid etching, while the etched carbon fiber surface is hydrophilic and could provide nucleation sites for the growth of NiCo₂O₄ nanowires.

After carbonized at 800 °C, it can be seen in the Fig. 2d, e that the NiCo₂O₄ nanowires are reduced into NiCo alloy nanoparticles with the diameter of 100–500 nm. They are closely anchored on the surface of CFs, implying the strong interaction between the decorated nanoparticles and CFs. In addition, the surface of the CF@NiCo composites became evidently rough and there are some grooves along the fiber axial direction. Moreover, it can be surprisingly observed that there are many pores on the surface and some NiCo alloy nanoparticles are partially embedded in the matrix of the CFs. This is mainly because the NiCo₂O₄ nanowire possess high surface energy and the NiCo alloy nanoparticles exhibit strong magnetic interaction among them, which makes NiCo₂O₄ nanowires melt and transform into the 3D NiCo nanoparticles to decrease the energy of the system.[39] Moreover, the carbon layer on the surface that connected with the NiCo₂O₄ nanowires was consumed gradually during the reduction process under the carbon thermal conditions, making the NiCo nanoparticles further penetrated into the CF matrix gradually with consuming more carbon substrate.

Elemental mappings of the CF@NiCo₂O₄ and CF@NiCo composites have also been performed to investigate the element distributions of the samples, and the results are shown in the Fig. 2. Furthermore, the

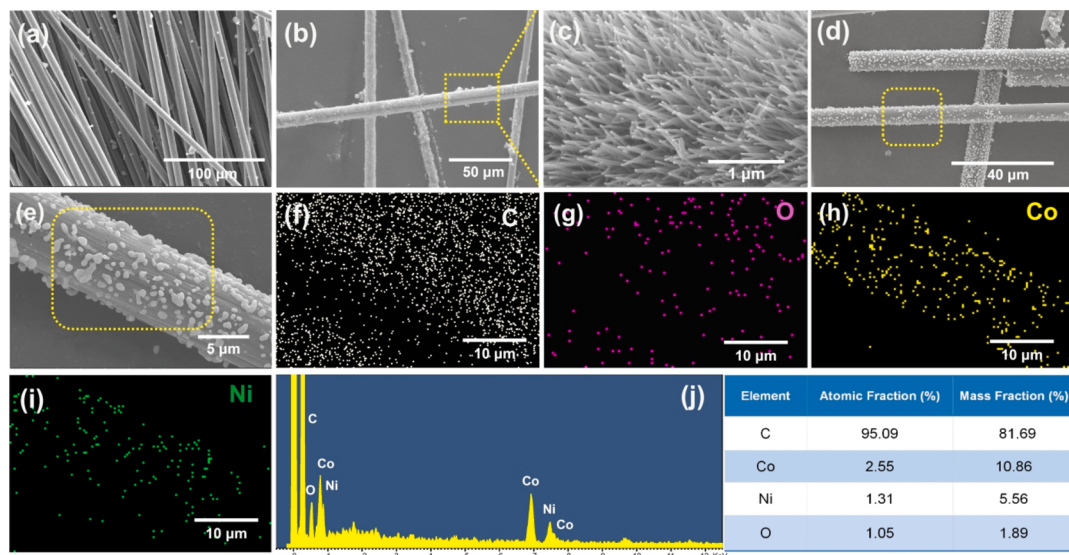


Fig. 2. Morphological and structural characterization: (a) SEM image of the pure carbon fibers. (b, c) NiCo_2O_4 nanoarrays decorated on the carbon fibers. (d, e) SEM image of CF@NiCo at different magnifications. (f-i) EDS images and the element mapping analysis of CF@NiCo. (j) EDS pattern and element content analysis of CF@NiCo.

element content is analyzed by the element surface scanning graph and the element content is distinguished by color. It could be found that the Co and Ni elements are evenly distributed on the CFs, and the element content ratio of Co/Ni is close to 2:1, which is consistent with the chemical structure of the derived NiCo_2O_4 nanowires. The corresponding elemental spectrum is listed in Fig. 2f and followed by the relative element content analysis. It can be seen that the CF@NiCo is mainly composed of C, Co, Ni and O elements. Among them, C element content is the highest, followed by the Co, Ni and O element. The Fig. 2e is the original image of CF@NiCo composites for elemental mapping and following four colored images are corresponding to C, O, Co and Ni elements, respectively. The Co and Ni are distributed homogeneously

along the CF. Moreover, after treated at 800°C, the O element content was significantly reduced and completely converted into metal alloys.

3.2. Structural characterization of CF@NiCo composites

The crystal structures of the samples have been further determined by XRD, as shown in Fig. 3a. It can be observed from the pattern of CF@ NiCo_2O_4 composites that there are five obvious characteristic peaks located at $2\theta = 31.1^\circ, 36.7^\circ, 44.6^\circ, 59.1^\circ$ and 64.8° , respectively, which are consistent with the standard card of NiCo_2O_4 (JCPDSNo.20-0781) and assigned to inverse cubic spinel structure of NiCo_2O_4 [40]. Moreover, the crystal structure of the composite CF@ NiCo_2O_4 has been

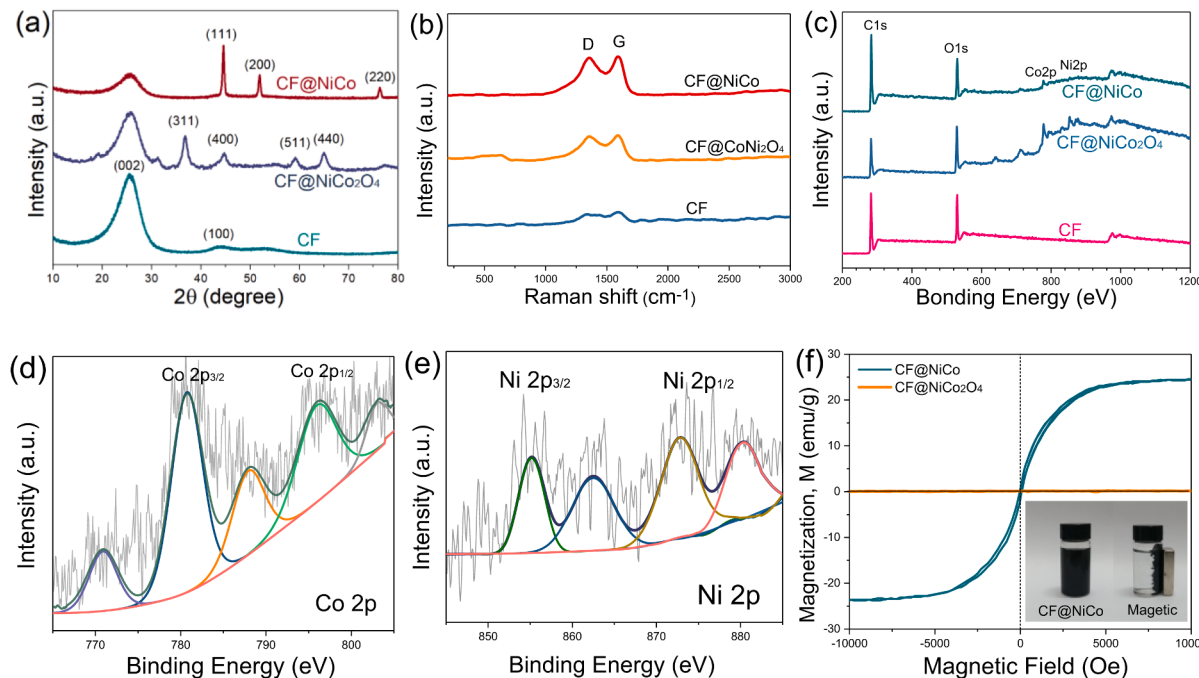


Fig. 3. Structural characterization. (a, b) The XRD patterns and Raman spectra of the pure CF, $\text{CF}@\text{NiCo}_2\text{O}_4$ and CF@NiCo composites. (c-e) The XPS analysis of pure CF, $\text{CF}@\text{NiCo}_2\text{O}_4$, CF@NiCo and Ni, Co elements. (f) Magnetic hysteresis loops of CF@NiCo and $\text{CF}@\text{NiCo}_2\text{O}_4$, the inset shows CF@NiCo dispersion in the DI water and its magnetism.

obviously changed after being annealed at 800°C, and there are obvious diffraction peaks at $2\theta = 44.3^\circ$, 51.6° and 76.2° , which are assigned to the (111), (200) and (220) planes of NiCo alloy with face centered cubic (fcc) structure. Moreover, the diffraction peaks of the samples are obvious, indicating the crystallinity of NiCo_2O_4 nanowires and NiCo alloy nanoparticles. Furthermore, the amorphous peak at $2\theta = 25.5^\circ$ can be detected for all CFs, CF@ NiCo_2O_4 and CF@NiCo samples, which corresponding to the (002) crystal plane of turbostratic graphitic structure, indicating a complex mixture of crystalline graphitic phase and amorphous carbon substrate of the CFs.

Fig. 3b displays the Raman spectra of pure CFs and magnetic composite carbon fibers. The D band centered at 1335 cm^{-1} – 1345 cm^{-1} represents the disordered/defective structure of sp^3 carbon atoms, and the G band near the central position of 1581 cm^{-1} – 1590 cm^{-1} represents the ordered structure of sp^2 carbon atoms. The D/G ratio is usually used to evaluate the graphitization degree of carbon materials. After carbonized at 800 °C, the ratio of I_D/I_G slightly increased from 1.0 to 1.06, indicating that the heating treatment repaired the structural defects, and the graphitization degree and order structure part were increased within the CFs.

The bonding configurations and surface chemical states of as-prepared CF@ NiCo_2O_4 and CF/NiCo composites were examined by X-ray photoelectron spectroscopy (XPS). The full survey XPS spectra (Fig. 3c) reveals the presence of C, O, Co and Ni elements. The high-resolution XPS spectra of Co 2p and Ni 2p of the CF@NiCo are shown in the Fig. 3d and e. It could found that there are two main peaks in the Co 2p region, and the binding energies at 780.9 eV and 796.4 eV are to Co 2p_{3/2} and Co 2p_{1/2}, respectively, which are Co²⁺ in the oxidation state [41,42]. Similarly, in the Ni 2p region, the peaks at binding energy

of 873.1 eV and 855.4 eV are Ni²⁺ in the oxidation state for Ni 2p_{1/2} and Ni 2p_{3/2}, suggesting the surface oxidation of the obtained NiCo alloy nanoparticles.

The magnetic properties of CF@ NiCo_2O_4 and CF/NiCo composites were analyzed. Fig. 3f shows the corresponding magnetization hysteresis loop under the magnetic field range of -10 – $+10 \text{ kOe}$ at 300 k. It is found that the magnetic property of CF@ NiCo_2O_4 was not detected due to the too weak magnetism and low relative weight content of the NiCo_2O_4 nanowires. The CF@NiCo shows typical paramagnetism and the saturation magnetization value (H_s) of 24.6 emu/g, and the coercivity of CF@NiCo reached 125 Oe. This prominent magnetic performance can be ascribed to the spherical NiCo alloy with great shape anisotropy, which is beneficial to the improvement of its coercivity. Besides, the CF@NiCo is extremely sensitive to external magnetic field (Fig. 3f), its aqueous dispersion could be completely separated immediately under the stimulation of the external magnetic field, showing high magnetic separation efficiency.

3.3. Mechanical properties of composite films

The uniform morphology and homogeneous internal structure are the key factors that affecting the comprehensive properties of the composite films. As illustrated in Fig. 3f, the chopped CFs could be easily dispersed in the water under stirring, which is beneficial to fabricate homogeneous composite films. Afterward, the timely vacuum-assisted filtration is necessary to avoid the settlement of CFs. After adding the polyamide solution followed by hot-pressing, the dense films with excellent mechanical properties were obtained. Fig. 4g,h show the upper surface and cross-section of the CF fabrics that were fixed with a small

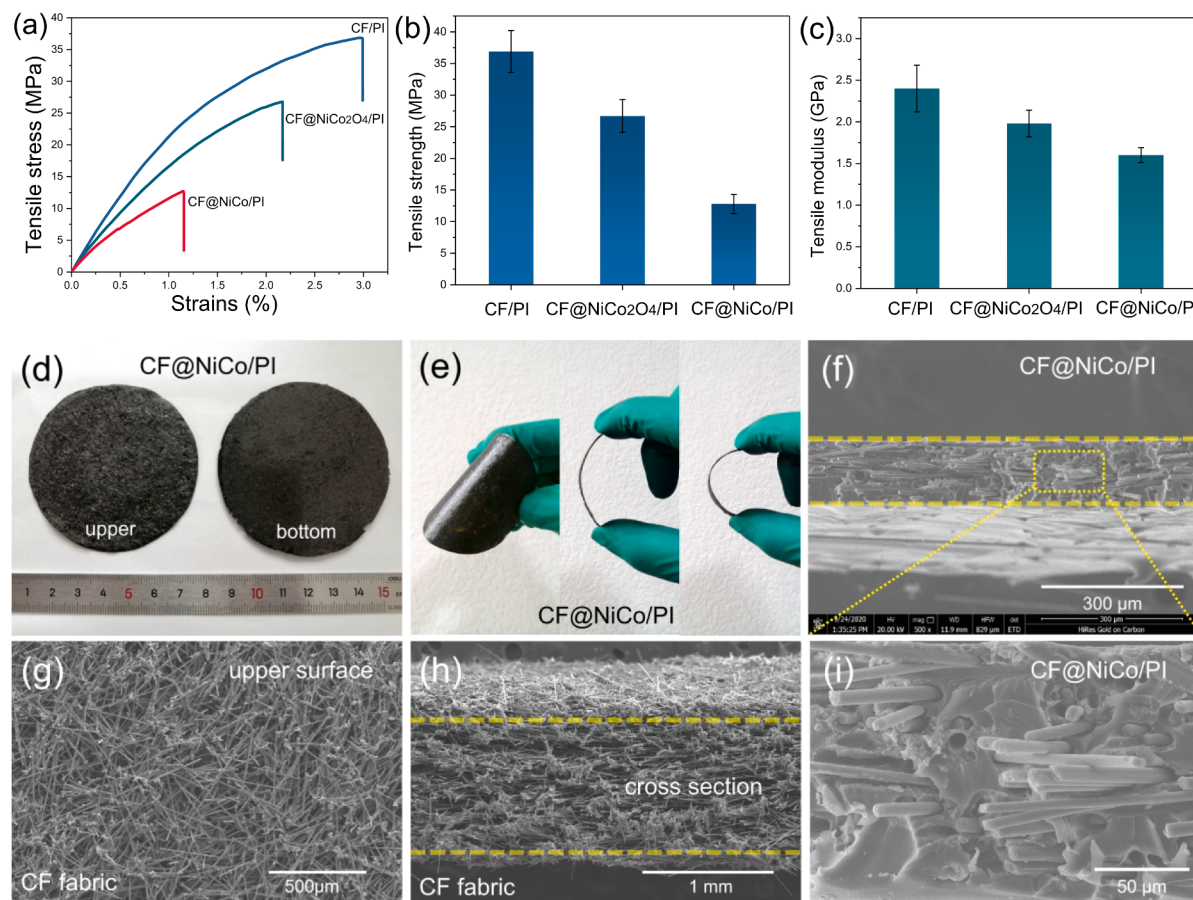


Fig. 4. (a) Engineering tensile stress-strain curves of the CF/PI, CF@ NiCo_2O_4 /PI and CF@NiCo/PI films. (b, c) The tensile strength and modulus of the composite films. (d, e) The optical image and the flexibility of CF@NiCo/PI films. (g, h) The upper surface and the cross-section of CF fabrics. (f, i) SEM image of the fractured surface of CF@NiCo/PI films.

amount of PI resin. As can be seen, the chopped CFs were assembled into uniform fabrics after filtration. Moreover, a three-dimensional overlapping frame network could be formed by settlement of the CFs, which is beneficial to obtain the composite materials with excellent mechanical performance.

The CF@NiCo₂O₄ and CF@NiCo fabrics were prepared with the same method, and an electrical/magnetic three-dimensional structure with excellent conductivity was obtained. Fig. 4d is the digital image of CF@NiCo/PI film after encapsulating with polyimide resin. As shown here, the surface of the obtained film is flat and uniform. The encapsulation with PI resin endows the composite films with favorable mechanical properties. The flexibility of CF@NiCo/PI films were also tested (Fig. 4e). The resultant composite films exhibit excellent mechanical flexibility and could withstand repeated bending without damage, which can be ascribed to the excellent flexibility and strength of the polyimide substrate.

Mechanical properties are of great significance for practical application of the EMI shielding materials. The mechanical properties of the PI encapsulated composite films were measured and the results are shown in Fig. 4a–c. The composite CF/PI films exhibit high tensile strength of 57.7 MPa with the corresponding modulus of 2.79 GPa. The CFs could act as the reinforcement to enhance the mechanical properties of the PI substrate via stress transmission.

In comparison, the CF@NiCo/PI and CF@NiCo₂O₄/PI composite films show decreased mechanical properties. The tensile strength of CF@NiCo₂O₄/PI and CF@NiCo/PI composite films are measured to be 26 MPa and 12 MPa, respectively. The decrease in tensile strength is mainly caused by the acid treatment and pyrolysis procedures. Lots of

defects were generated on the surface and within the substrate of the CFs, which brought obvious negative effects on the mechanical properties of the composite films. It counteracts the positive effect induced by the high bonding force between the PI resin and rough surface of the CFs. Especially after treating at 800 °C, the carbon substrate of the CFs was consumed by the carbon thermal reaction with the NiCo₂O₄ nanowires, and a large number of gullies and holes were generated on the surface of CFs, leading to the decline of the mechanical properties of CF@NiCo films. This finally results in the attenuation of overall mechanical properties of CF@NiCo/PI composite films. Even so, the mechanical properties of the composite films are still favorable for the practical applications. Generally, the polyimide exhibits excellent thermal resistance performance, chemical stability [43], combined with the good mechanical properties, ensuring the durable application of as-prepared composite films in various complex or harsh environments.

3.4. Electrical and heating performances of composite films

The heating performance of the composite films were also explored. Fig. 5a shows the time–temperature curves of the CF@NiCo/PI-0.6 film at a constant voltage from 1.0 V to 5.0 V. At the low input voltage of 1 V, the surface temperature of CF@NiCo/PI-0.6 film was heated from 27.5 °C to 33.9 °C. As the input voltage increased to 2.0 V, the surface temperature enhanced gradually and the temperature eventually stabilized at 50.6 °C finally. Furthermore, the steady-state saturated temperature enhances further with gradient increase of the input voltages owing to the higher passing current. At the supplied voltage of 5.0 V, the surface temperature sharply reached to about 100 °C within 20 s. As shown in

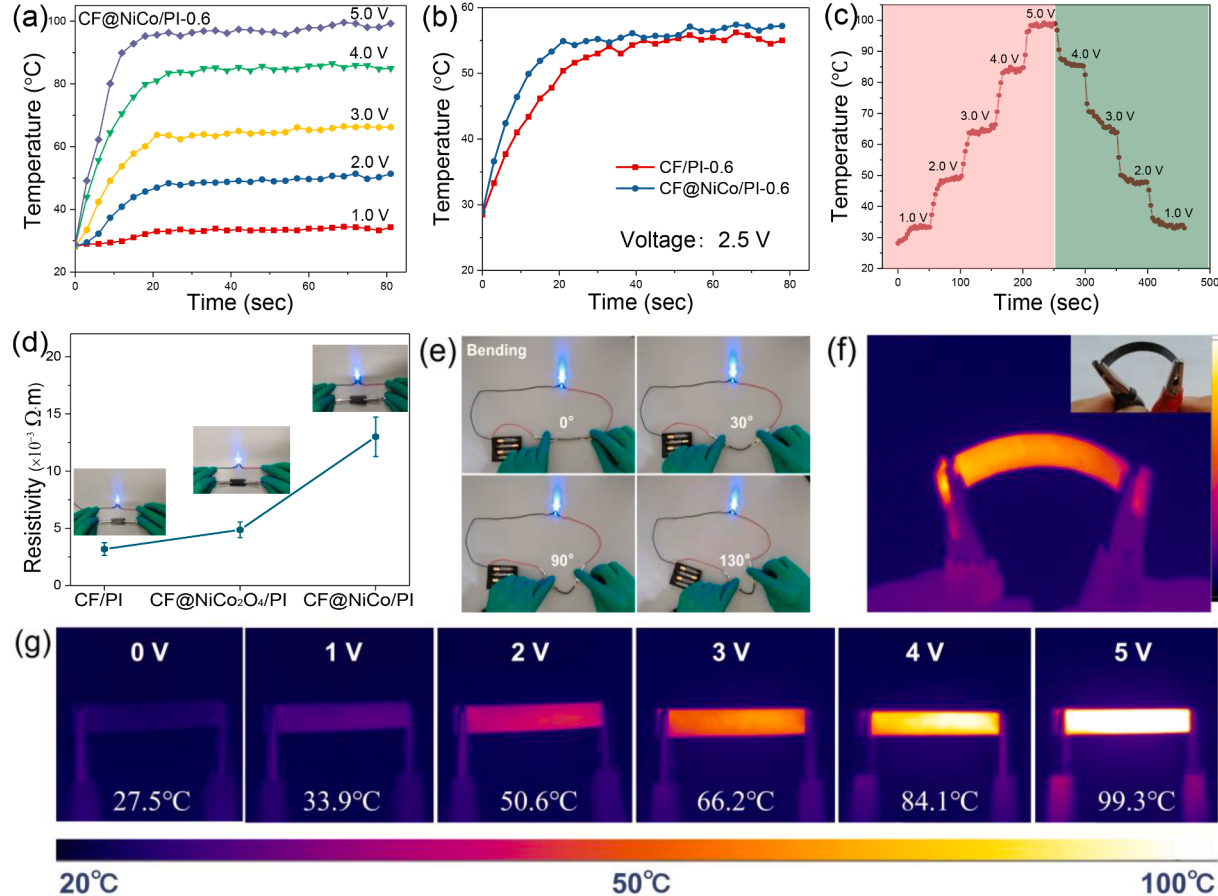
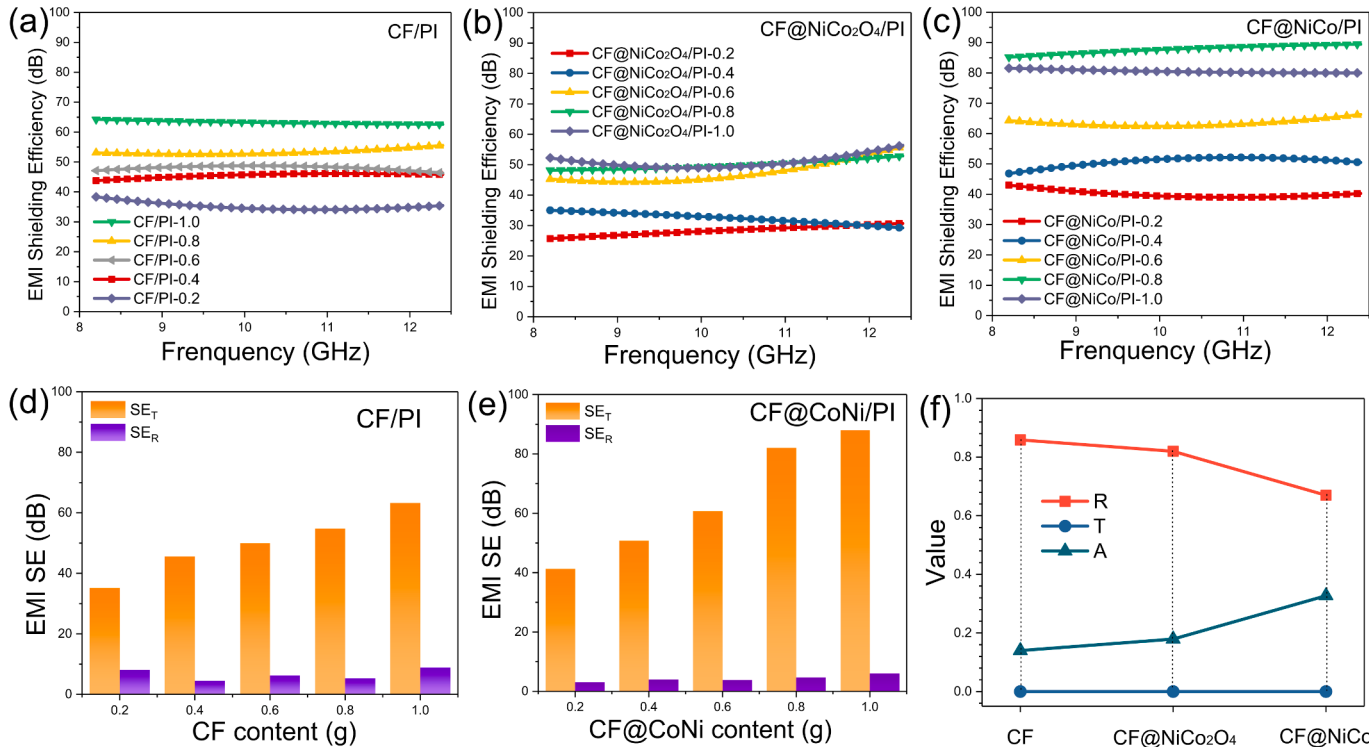


Fig. 5. (a and b) Time-dependent surface temperatures of the composite films with different supplied voltages, respectively. (c and g) Tailored surface temperatures of the electrical heaters upon gradually changed voltages. (d and e) The resistance of the composite films and electrical conductivity upon bending. (f) The heating performance of the CF@NiCo/PI-0.6 upon bending.

the Fig. 5g, the IR camera recorded the corresponding surface temperatures with variation of gradient supplied voltages. In addition, Fig. 5f shows that the flexible composite film also has uniform heating characteristics during the large angle bending. When the supplied voltage decreased gradually, the surface temperatures of the composite films can also react rapidly with the variation of the voltage, indicating the obvious heat dissipation effect of composite films. The results demonstrate that the composite films with high mechanical strength and fast temperature-voltage response characteristics can be widely used in electronic components as thermal management materials.

Moreover, it can be seen from Fig. 5b that the heating efficiency of CF@NiCo/PI-0.6 film is higher than CF@NiCo₂O₄/PI-0.6 film at the same input voltage of 2.5 V. The CF@NiCo/PI-0.6 could reach the saturated temperature faster, and its final stable temperature is also higher than that of CF@NiCo₂O₄/PI-0.6 film. In general, the joule heating performance of the conductive composite materials is closely related to their resistivities. The resistivity of the composite films derived from CF, CF@NiCo₂O₄ and CF@NiCo after encapsulation were measured and the results are shown in the Fig. 5d. The average resistivity of CF/PI is $3.2 \times 10^{-3} \Omega \text{ m}$, indicating that CF/PI film still maintains excellent conductivity after being encapsulated with polyimide resin. Due to the coverage of the NiCo₂O₄ nanoarray on the CF, the average resistance of CF@NiCo₂O₄/PI films declines slightly. Meanwhile, the average resistance of the CF@NiCo films rises sharply to $13.2 \times 10^{-3} \Omega \text{ m}$. This mainly because the continuous conductive path is destroyed and a large number of pores are generated within the carbon matrix after pyrolysis at 800 °C. In addition, the interface between NiCo alloy nanoparticles and carbon fibers will also hinder the charge movement, resulting in more Joule heat. However, the as-prepared composite films exhibit extremely low resistance on the whole, and even if the composite film was bent at a large angle of 130°, the brightness of the LED lamp almost did not change (Fig. 5e). The excellent electrical conductivity of the composite films is beneficial to achieve the ideal heating effect at low voltages and ensure the safety of the functional component.



3.5. Electromagnetic properties and EMI shielding performances

The EMI shielding performances of prepared composite films were tested in the X band. Fig. 6a–c show the EMI shielding performance of the CF/PI, CF@NiCo₂O₄/PI and CF@NiCo/PI composite films, respectively. It could be found that the CF/PI films exhibit excellent EMI shielding performances. The average EMI SE of the CF/PI-0.2 film is 36 dB on average in the X band, which is a bit higher than the standard of commercial EMI shielding materials (30 dB). Moreover, the thickness of CF/PI films can be adjusted by loading different contents of CFs. While the CF loading raised to 1.0 g, the EMI SE of CF/PI-1.0 film could reach 4 dB with a thickness of ~1.1 mm. This superior EMI shielding performance of the pristine CF/PI film is closely associated with the internal 3D conductive structural network that formed by mutually contacted CFs.

Fig. 6b shows the EMI shielding performance of the CF@NiCo₂O₄/PI films. It is clearly observed that the EMI shielding performances of the CF@NiCo₂O₄/PI films decreased in comparison with the CF/PI film. Even for the CF@NiCo₂O₄/PI-1.0 film with the thickness of ~1.1 mm, the EMI SE was only ~50 dB, which is relatively lower than that of CF/PI-1.0 film with almost the same thickness. This result is mainly caused by the weak electrical conductivity and magnetic response of the NiCo₂O₄ nanowires [44,45]. The needle-like NiCo₂O₄ nanowires almost completely covered the surface of the CFs, resulting in the destruction of the original conductive path of the CF fabric. High conductivity is the premise to realize efficient EMI shielding performance. Therefore, the reflection loss and conductive loss of the CF@NiCo₂O₄/PI films were significantly decreased in comparison with the CF/PI films, resulting in a obvious reduction in the total EMI shielding efficiency.

It can be seen from Fig. 6c that the EMI shielding performance of the CF@NiCo/PI films is much higher than those of CF/PI and CF@NiCo₂O₄/PI films. Even for the CF@NiCo/PI-0.2 film with the thickness of only 0.22 mm, its average EMI SE could reach 40 dB on average and 99.99% of EM waves were shielded. Moreover, with increasing the CF@NiCo composites loading, the EMI SE of the CF@NiCo/PI films was increased significantly. The EMI SE of the CF@NiCo/PI-1.0 film reached

Fig. 6. EMI shielding performances: (a–c) EMI SE of CF/PI, CF@NiCo₂O₄/PI and CF@NiCo/PI composite films with different thicknesses. (d, e) SE_R and SE_A of CF/PI and CF@NiCo/PI composite films with different thicknesses. (f) Comparison of the R, T, A values of composite films at X-band.

up to 87 dB on average while the thickness of the sample was just 1.08 mm, which is significantly superior to the reported materials such as carbon-based and metal materials. Furthermore, the average density of the CF@NiCo-1.0 film was measured to be $\sim 0.5 \text{ g cm}^{-3}$, indicating that the specific shielding effectiveness (SSE) and SSE/t were $167.3 \text{ dB cm}^3 \text{ g}^{-1}$ and $1549.2 \text{ dB cm}^3 \text{ g}^{-1}$, respectively.

In order to analyze the EMI shielding mechanisms of the composite films, the effects of chemical structure and morphology of the nanoparticles on EMI shielding performances were explored. The contributions of the reflection part (SE_R) and absorption part (SE_A) to the total electromagnetic shielding efficiency (SE_T) of flexible composite films were analyzed as well. As shown in the Fig. 6d and e, the SE_T and SE_A values of all samples display an increasing trend with increasing the CFs loading, and the SE_A values are much higher than the corresponding SE_R values. Especially for the CF@NiCo/PI films, with increasing the content of the CF@NiCo and thickness of the CF@NiCo/PI films, the SE_R maintained at low constant values and the relative values of the SE_T and SE_R improved gradually. It is evident that the increased SE_T value is entirely based on the increase of the SE_A . For example, the SE_A and SE_R values of the CF@NiCo/PI-1.0 film are 80.9 dB and 6.0 dB, respectively, which is superior to the previously reported data with the similar materials thickness.

Furthermore, the reflectivity (R), transmittance (T) and absorption coefficient (A) of the CF/PI-1.0, CF@NiCo₂O₄/PI-1.0 and CF@NiCo/PI-1.0 samples were calculated through the parameters of input reflection

S11, reverse transmission S12, forward transmission S21 and output reflection S22. The T values of these three composite films are close to zero, which shows that the flexible composite films could effectively shield the incident EM waves, and very few EM waves could pass through the films. As shown in the Fig. 6f, with increasing the treatment temperature, the R of the as-prepared composite films decreases and the A increases correspondingly. The A values of the CF/PI-1.0, CF@NiCo₂O₄/PI-1.0 and CF@NiCo/PI-1.0 films are 0.14, 0.18 and 0.33, respectively. When the NiCo₂O₄ nanowires were converting into NiCo alloy nanoparticles, the A value of the CF@NiCo/PI films improved sharply, indicating the high EM waves absorption capacity of the CF@NiCo/PI films. Moreover, in comparison with the pure CF/PI, the slight improvement in the A of the CF@NiCo₂O₄/PI can be ascribed to the certain dielectric loss and magnetic loss of NiCo₂O₄ nanowires. Although the decorated NiCo₂O₄ destroys the conductive path of the CF matrix, but it enhances the dielectric loss effect of the CF matrix [46,47]. This synergistic effect improves the absorption coefficient of CF@NiCo₂O₄/PI film, which is consistent with the variation tendency of the SE_R and SE_A of the CF/PI and CF@NiCo₂O₄/PI films.

Moreover, the weight of the CF@NiCo/PI-1.0 film was measured to be 2.4 g, means the content of CF@NiCo is about 41 wt%. Thus, the complex dielectric permittivity and magnetic permeability are experimentally and theoretically simulated using coaxial method with the sample consisting of CF@NiCo: paraffin of 4:6. Fig. 7a, b show the relative complex permittivity and permeability in the frequency range of

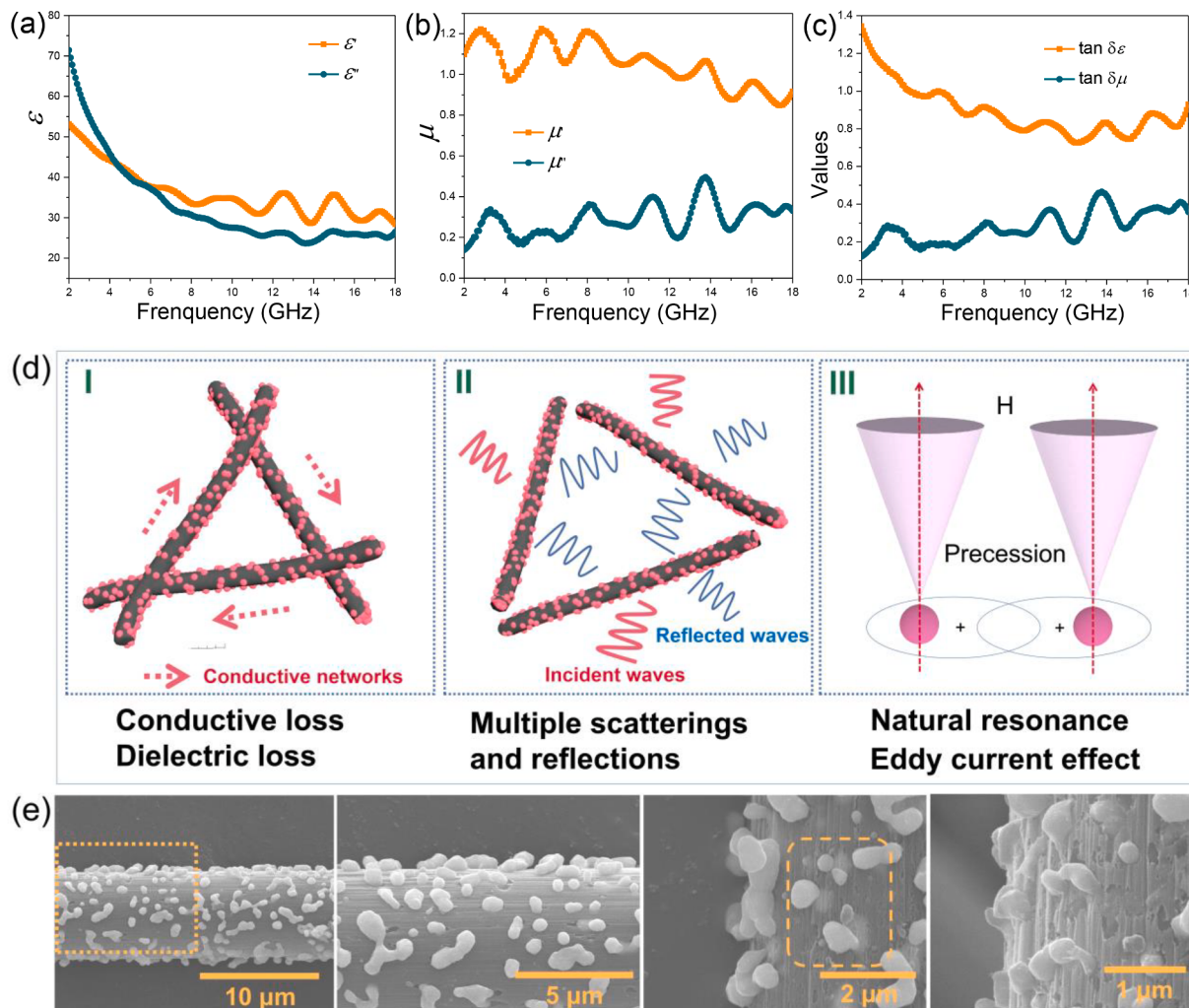


Fig. 7. (a–c) Real part and imaginary part of the permittivity, permeability, $\tan \epsilon$ and $\tan \mu$ vs frequency of CF@NiCo/PI films. (d) Schematic illustration of feasible EMI shielding mechanism for CF@NiCo/PI films. (e) The morphology of CF@NiCo composites.

2–18 GHz. Specifically, the ϵ' and ϵ'' of the CF@NiCo are mainly located in the range of 25–35, which is moderate for the EMI shielding materials. According to Fig. 7b, the μ'' and $\tan \delta_\mu$ increase with increasing frequency in 2–18 GHz. Moreover, the peaks at 8.2 and 11.3 GHz are the characteristic peaks of the magnetic resonance, indicating the strong magnetic loss capability, which may be caused by the natural resonance, eddy current loss and exchange resonance of NiCo nanoparticles [48–50]. The relative high $\tan \delta_\mu$ value also reveals the strong magnetic loss capacity of the CF@NiCo/PI films.

According to the analysis mentioned above, the feasible EM shielding mechanism is proposed in Fig. 7d. When EM waves contacts with the surface of the composite film, few of EM waves are reflected, and most EM waves could continue to transmit forward due to the large number of gaps between the CFs on the surface and favorable impedance matching of the composite films. The incident EM waves can be reflected for multiple times within the three-dimensional conductive network, and most EM waves could be converted into the heat energy due to the dielectric loss of the CFs. On the other hand, the plenty of NiCo alloy nanoparticles with excellent conductivity and magnetic loss are tightly anchored on the surface or embedded in the CFs, providing a channel for electron transmission and causing conductive loss for the CF@NiCo/PI. Moreover, the raised NiCo nanoparticles and large number of surface defects generated by etching and pyrolysis could effectively improve the absorption and dissipation of microwaves. It is noteworthy that, the porous electrical/magnetic composite substrate trigger wider concerns in the EMI shielding area, because the porous structure could allow the microwaves to enter the materials as much as possible, which is equivalent to impedance matching [51,52]. On the other hand, the porous structure could induce multiple reflection and scattering of the incident EM waves within the materials, which prolongs the transmission path of incident EM microwaves and improve the probability of the incident EM energy to be scattered and dissipated the EM energy into Joule heat.

Besides, the NiCo alloy nanoparticles exhibit natural magnetic loss for incident EM waves, [53,54] which is mainly due to the fact that the precession frequency of magnetic NiCo alloy nanoparticles is close to the frequency of EM waves. The generated natural resonance makes the incident EM waves were absorbed or attenuated again, leading to the improved absorption loss capacity and the EMI shielding performances of CF@NiCo/PI films. Furthermore, the increase in thickness of the composite films could prolong the transmission distance of the incident EM waves within the 3D electrical/magnetic network, which promotes the multiple absorption and reflection of incident EM waves [55]. Therefore, the incident EM waves could be almost completely attenuated through these synergistic effects of conductivity loss, dielectric loss and magnetic loss. The EM energy was transferred into the thermal energy finally and thus achieving the excellent EMI shielding performance with outstanding absorption characteristics.

4. Conclusions

In summary, we have developed a series of flexible CF@NiCo/PI composite films with low EM reflection characteristics via pyrolysis and vacuum-assistant filtration approach. The influences of morphology and chemical structures of the carbon fiber composites on EMI shielding performances of CF@NiCo/PI films were explored. The EMI SE of the CF@NiCo/PI reached to as high as 87 dB on average in the X band (8.2–12.4 GHz) with the thickness of only 1.08 mm, and the corresponding SE_R and SE_A are 81 dB and 6 dB, respectively. This highly efficient EM wave absorption can be attributed to the synergistic mechanisms of dielectric loss and magnetic loss of the NiCo alloy and porous CF matrix, which greatly enhance the well-matched impedance and absorption capacity of the incident EM waves. Moreover, the EMI shielding performance of the CF@NiCo/PI films can be tailored by loading different amounts of CF@NiCo composites to meet various practical requirements. In addition, the prepared CF@NiCo/PI films present superior flexibility, tensile strength (12 MPa) and modulus (264

MPa) and electrical conductivity ($13.2 \times 10^{-3} \Omega \text{ m}$). The prepared flexible composite films have broad application prospects in the fields of microelectronics and portable communication fields as EMI shielding and heat management materials.

Declaration of Competing Interest

The authors declare that they have no known competing financial interests or personal relationships that could have appeared to influence the work reported in this paper.

Acknowledgments

This study was supported by National Natural Science Foundation of China (51903145), the Postgraduate Innovation Foundation of Xi'an Polytechnic University (CHX2020037), Scientific Research Program Funded by Shaanxi Provincial Education Department (21JK0657) and Shenghong Scientific Research Projects of National Advanced Function Fiber Innovation Center (2020-fx020009).

References

- [1] D. Jiang, V. Murugadoss, Y. Wang, J. Lin, T. Ding, Z. Wang, Q. Shao, C. Wang, H. Liu, N. Lu, Electromagnetic interference shielding polymers and nanocomposites-a review, *Polym. Rev.* 59 (2019) 280–337.
- [2] A.K. Singh, A. Shishkin, T. Koppel, N. Gupta, A review of porous lightweight composite materials for electromagnetic interference shielding, *Compos. B Eng.* 149 (2018) 188–197.
- [3] J. Liu, H.B. Zhang, X. Xie, R. Yang, Z. Liu, Y. Liu, Z.Z. Yu, Multifunctional, superelastic, and lightweight MXene/polyimide aerogels, *Small* 14 (2018) 1802479.
- [4] F. Shahzad, M. Alhabeb, C.B. Hatter, B. Anasori, S.M. Hong, C.M. Koo, Y. Gogotsi, Electromagnetic interference shielding with 2D transition metal carbides (MXenes), *Science* 353 (2016) 1137–1140.
- [5] Y. Li, X. Tian, S.P. Gao, L. Jing, K. Li, H. Yang, F. Fu, J.Y. Lee, Y.X. Guo, J.S. Ho, Reversible crumpling of 2D titanium carbide (MXene) nanocoatings for stretchable electromagnetic shielding and wearable wireless communication, *Adv. Funct. Mater.* 30 (2020) 1907451.
- [6] J. Liu, Z. Liu, H.B. Zhang, W. Chen, Z. Zhao, Q.W. Wang, Z.Z. Yu, Ultrastrong and highly conductive MXene-based films for high-performance electromagnetic interference shielding, *Adv. Electron. Mater.* 6 (2020) 1901094.
- [7] Z. Ma, S. Kang, J. Ma, L. Shao, Y. Zhang, C. Liu, A. Wei, X. Xiang, L. Wei, J. Gu, Ultraflexible and mechanically strong double-layered aramid nanofiber-Ti3C2T x MXene/silver nanowire nanocomposite papers for high-performance electromagnetic interference shielding, *ACS Nano* 14 (2020) 8368–8382.
- [8] X. Liu, Y. Li, X. Sun, W. Tang, G. Deng, Y. Liu, Z. Song, Y. Yu, R. Yu, L. Dai, J. Shui, Off/on switchable smart electromagnetic interference shielding aerogel, *Matter* 4 (2021) 1735–1747.
- [9] Q. Wei, S. Pei, X. Qian, H. Liu, Z. Liu, W. Zhang, T. Zhou, Z. Zhang, X. Zhang, H. M. Cheng, Superhigh electromagnetic interference shielding of ultrathin aligned pristine graphene nanosheets film, *Adv. Mater.* 32 (2020) 1907411.
- [10] T. Yun, H. Kim, A. Iqbal, Y.S. Cho, G.S. Lee, M.K. Kim, S.J. Kim, D. Kim, Y. Gogotsi, S.O. Kim, Electromagnetic shielding of monolayer MXene assemblies, *Adv. Mater.* 32 (2020) 1906769.
- [11] D. Wanasinghe, F. Aslani, G. Ma, D. Habibi, Review of polymer composites with diverse nanofillers for electromagnetic interference shielding, *Nanomaterials* 10 (2020) 541.
- [12] L. Liang, P. Xu, Y. Wang, Y. Shang, J. Ma, F. Su, Y. Feng, C. He, Y. Wang, C. Liu, Flexible polyvinylidene fluoride film with alternating oriented graphene/Ni nanochains for electromagnetic interference shielding and thermal management, *Chem. Eng. J.* 395 (2020), 125209.
- [13] X. Zhang, J. Xu, H. Yuan, S. Zhang, Q. Ouyang, C. Zhu, X. Zhang, Y. Chen, Large-scale synthesis of three-dimensional reduced graphene oxide/nitrogen-doped carbon nanotube heteronanostructures as highly efficient electromagnetic wave absorbing materials, *ACS Appl. Mater. Interfaces* 11 (2019) 39100–39108.
- [14] L. Wang, B. Wen, X. Bai, C. Liu, H. Yang, NiCo alloy/carbon nanorods decorated with carbon nanotubes for microwave absorption, *ACS Appl. Nano Mater.* 2 (2019) 7827–7838.
- [15] R.S. Yadav, I. Kurikta, J. Vilcakova, D. Skoda, P. Urbánek, M. Machovsky, M. Masar, L. Kalina, J. Havlica, Lightweight NiFe₂O₄-reduced graphene oxide-elastomer nanocomposite flexible sheet for electromagnetic interference shielding application, *Compos. B Eng.* 166 (2019) 95–111.
- [16] J. Xu, L. Xia, J. Luo, S. Lu, X. Huang, B. Zhong, T. Zhang, G. Wen, X. Wu, L. Xiong, High-performance electromagnetic wave absorbing CNT/SiC composites: synthesis, tuning, and mechanism, *ACS Appl. Mater. Interfaces* 12 (2020) 20775–20784.
- [17] I. Arif, Y. Bhattacharjee, O. Prakash, M. Sahu, S. Suwas, S. Bose, Tunable CoNi microstructures in flexible multilayered polymer films can shield electromagnetic radiation, *Compos. B Eng.* 177 (2019), 107283.

- [18] Q. Liu, X. He, C. Yi, D. Sun, J. Chen, D. Wang, K. Liu, M. Li, Fabrication of ultra-light nickel/graphene composite foam with 3D interpenetrating network for high-performance electromagnetic interference shielding, *Compos. B Eng.* 182 (2020), 107614.
- [19] Y. Li, B. Shen, X. Pei, Y. Zhang, D. Yi, W. Zhai, L. Zhang, X. Wei, W. Zheng, Ultrathin carbon foams for effective electromagnetic interference shielding, *Carbon* 100 (2016) 375–385.
- [20] B. Shen, W. Zhai, M. Tao, J. Ling, W. Zheng, Lightweight, multifunctional polyetherimide/graphene@ Fe_3O_4 composite foams for shielding of electromagnetic pollution, *ACS Appl. Mater. Interfaces* 5 (2013) 11383–11391.
- [21] J. Liang, Y. Gu, M. Bai, S. Wang, M. Li, Z. Zhang, Electromagnetic shielding property of carbon fiber felt made of different types of short-chopped carbon fibers, *Compos. A Appl. Sci. Manuf.* 121 (2019) 289–298.
- [22] M. Arjmand, K. Chizari, B. Krause, P. Pötschke, U. Sundararaj, Effect of synthesis catalyst on structure of nitrogen-doped carbon nanotubes and electrical conductivity and electromagnetic interference shielding of their polymeric nanocomposites, *Carbon* 98 (2016) 358–372.
- [23] X. Fan, G. Zhang, J. Li, Z. Shang, H. Zhang, Q. Gao, J. Qin, X. Shi, Study on foamability and electromagnetic interference shielding effectiveness of supercritical CO_2 foaming epoxy/rubber/MWCNTs composite, *Compos. A Appl. Sci. Manuf.* 121 (2019) 64–73.
- [24] Q. Gao, G. Zhang, X. Fan, H. Zhang, Y.u. Zhang, F. Huang, R. Xiao, X. Shi, J. Qin, Enhancements of foamability, electromagnetic interference shielding and mechanical property of epoxy microcellular composite foam with well-dispersed f-MWCNTs, *Compos. A Appl. Sci. Manuf.* 138 (2020) 106060.
- [25] Z. Ma, S. Kang, J. Ma, L. Shao, A. Wei, C. Liang, J. Gu, B. Yang, D. Dong, L. Wei, Z. Ji, High-performance and rapid-response electrical heaters based on ultraflexible, heat-resistant, and mechanically strong aramid nanofiber/Ag nanowire nanocomposite papers, *ACS Nano* 13 (2019) 7578–7590.
- [26] Z. Ma, A. Wei, Y. Li, L. Shao, H. Zhang, X. Xiang, J. Wang, Q. Ren, S. Kang, D. Dong, Lightweight, flexible and highly sensitive segregated microcellular nanocomposite piezoresistive sensors for human motion detection, *Compos. Sci. Technol.* 203 (2021), 108571.
- [27] J. Li, A. Wang, J. Qin, H. Zhang, Z. Ma, G. Zhang, Lightweight polymethacrylimide@ copper/nickel composite foams for electromagnetic shielding and monopole antennas, *Compos. A Appl. Sci. Manuf.* 140 (2021) 106144.
- [28] S. Li, Z. Xu, Y.u. Dong, D. Liu, G. Sui, Ni@nylon mesh/PP composites with a novel tree-ring structure for enhancing electromagnetic shielding, *Compos. A Appl. Sci. Manuf.* 131 (2020) 105798.
- [29] Y. Wang, W. Wang, X. Ding, D. Yu, Multilayer-structured Ni-Co-Fe-P/polyaniline/polymide composite fabric for robust electromagnetic shielding with low reflection characteristic, *Chem. Eng. J.* 380 (2020), 122553.
- [30] Z. Zeng, F. Jiang, Y. Yue, D. Han, L. Lin, S. Zhao, Y.B. Zhao, Z. Pan, C. Li, G. Nyström, Flexible and ultrathin waterproofer cellular membranes based on high-conjunction metal-wrapped polymer nanofibers for electromagnetic interference shielding, *Adv. Mater.* 32 (2020) 1908496.
- [31] R. Li, S. Wang, P. Bai, B. Fan, B. Zhao, R. Zhang, Enhancement of electromagnetic interference shielding from the synergism between Cu@Ni nanorods and carbon materials in flexible composite films, *Mater. Adv.* 2 (2021) 718–727.
- [32] B. Zhao, X. Li, S. Zeng, R. Wang, L. Wang, R. Che, R. Zhang, C.B. Park, Highly compressible polymer composite foams with thermal heating-boosted electromagnetic wave absorption abilities, *ACS Appl. Mater. Interfaces* 12 (2020) 50793–50802.
- [33] H. Zhang, G. Zhang, Q. Gao, M. Tang, Z. Ma, J. Qin, M. Wang, J.-K. Kim, Multifunctional microcellular PVDF/Ni-chains composite foams with enhanced electromagnetic interference shielding and superior thermal insulation performance, *Chem. Eng. J.* 379 (2020), 122304.
- [34] N. Zhang, X. Liu, Y. Huang, M. Wang, S. Li, M. Zong, P. Liu, Novel nanocomposites of cobalt ferrite covalently-grafted on graphene by amide bond as superior electromagnetic wave absorber, *J. Colloid Interface Sci.* 540 (2019) 218–227.
- [35] A.H. Hart, R. Koizumi, J. Hamel, P.S. Owuor, Y. Ito, S. Ozden, S. Bhowmick, S. A. Syed Amanulla, T. Tsafack, K. Keyshar, Velcro-inspired SiC fuzzy fibers for aerospace applications, *ACS Appl. Mater. Interfaces* 9 (2017) 13742–13750.
- [36] H. Zhang, G. Zhang, J. Li, X. Fan, Z. Jing, J. Li, X. Shi, Lightweight, multifunctional microcellular PMMA/ Fe_3O_4 @MWCNTs nanocomposite foams with efficient electromagnetic interference shielding, *Compos. A Appl. Sci. Manuf.* 100 (2017) 128–138.
- [37] H. Duan, H. Zhu, J. Gao, D.-X. Yan, K. Dai, Y. Yang, G. Zhao, Y. Liu, Z.-M. Li, Asymmetric conductive polymer composite foam for absorption dominated ultra-efficient electromagnetic interference shielding with extremely low reflection characteristics, *J. Mater. Chem. A* 8 (2020) 9146–9159.
- [38] A. Iqbal, P. Sambyal, C.M. Koo, 2D MXenes for electromagnetic shielding: a review, *Adv. Funct. Mater.* 30 (2020) 2000883.
- [39] H. Li, J. Liao, S. Feng, Y. Yu, X. Zhang, Z. Jin, Hollow CoNi alloy submicrospheres consisting of CoNi nanoplatelets: facile synthesis and magnetic properties, *Mater. Lett.* 67 (2012) 346–348.
- [40] J. Zhao, Z. Li, M. Zhang, A. Meng, Q. Li, Direct growth of ultrathin $\text{NiCo}_2\text{O}_4/\text{NiO}$ nanosheets on SiC nanowires as a free-standing advanced electrode for high-performance asymmetric supercapacitors, *ACS Sustainable Chem. Eng.* 4 (2016) 3598–3608.
- [41] D. Deng, Y. Tian, H. Li, L. Xu, J. Qian, J. Pang, B. Wang, Q.i. Zhang, H. Li, NiCo alloy nanoparticles encapsulated in multi-dimensional N-doped carbon architecture as efficient bifunctional catalyst for rechargeable zinc-air batteries, *J. Alloy. Compd.* 797 (2019) 1041–1049.
- [42] C. Yu, S. Hao, L. Lei, X. Zhang, Synthesis of NiCo alloy nanoparticle-decorated B, N-doped carbon nanosheet networks via a self-template strategy for bifunctional oxygen-involving reactions, *ACS Sustainable Chem. Eng.* 7 (2019) 14394–14399.
- [43] J. Li, N. Yu, Z. Jing, X. He, X. Shi, G. Zhang, Fabrication of rigid polyimide foams via thermal foaming of nadimide-end-capped polyester-amine precursor, *Polym. Bull.* 77 (2020) 5899–5912.
- [44] G. Li, H. Cai, X. Li, J. Zhang, D. Zhang, Y. Yang, J. Xiong, Construction of hierarchical $\text{NiCo}_2\text{O}_4@\text{Ni-MOF}$ hybrid arrays on carbon cloth as superior battery-type electrodes for flexible solid-state hybrid supercapacitors, *ACS Appl. Mater. Interfaces* 11 (2019) 37675–37684.
- [45] M. Wang, H. Zhang, J. Cui, S. Yao, X. Shen, T.J. Park, J.K. Kim, Recent advances in emerging nonaqueous K-ion batteries: from mechanistic insights to practical applications, *Energy Storage Mater.* 39 (2021) 305–346.
- [46] L. Liu, S. Yang, H. Hu, T. Zhang, Y. Yuan, Y. Li, X. He, Lightweight and efficient microwave-absorbing materials based on loofah-sponge-derived hierarchically porous carbons, *ACS Sustainable Chem. Eng.* 7 (2019) 1228–1238.
- [47] L. Huang, D. Chen, Y. Ding, S. Feng, Z.L. Wang, M. Liu, Nickel-cobalt hydroxide nanosheets coated on NiCo_2O_4 nanowires grown on carbon fiber paper for high-performance pseudocapacitors, *Nano Lett.* 13 (2013) 3135–3139.
- [48] S. Bai, X. Shen, G. Zhu, M. Li, H. Xi, K. Chen, In situ growth of $\text{Ni}_{x}\text{Co}_{100-x}$ nanoparticles on reduced graphene oxide nanosheets and their magnetic and catalytic properties, *ACS Appl. Mater. Interfaces* 4 (2012) 2378–2386.
- [49] F. Wu, P. Liu, J. Wang, T. Shah, M. Ahmad, Q. Zhang, B. Zhang, Fabrication of magnetic tubular fiber with multi-layer heterostructure and its microwave absorbing properties, *J. Colloid Interface Sci.* 577 (2020) 242–255.
- [50] N. Zhang, Y. Huang, M. Wang, X. Liu, M. Zong, Design and microwave absorption properties of thistle-like CoNi enveloped in dielectric Ag decorated graphene composites, *J. Colloid Interface Sci.* 534 (2019) 110–121.
- [51] J. Li, Y. Ding, N. Yu, Q. Gao, X. Fan, X. Wei, G. Zhang, Z. Ma, X. He, Lightweight and stiff carbon foams derived from rigid thermosetting polyimide foam with superior electromagnetic interference shielding performance, *Carbon* 158 (2020) 45–54.
- [52] X. Yan, X. Huang, B. Zhong, T. Wu, H. Wang, T. Zhang, N. Bai, G. Zhou, H. Pan, G. Wen, Balancing interface polarization strategy for enhancing electromagnetic wave absorption of carbon materials, *Chem. Eng. J.* 391 (2020), 123538.
- [53] J. Li, Y. Ding, Q. Gao, H. Zhang, X. He, Z. Ma, B. Wang, G. Zhang, Ultrathin and flexible biomass-derived C@CoFe nanocomposite films for efficient electromagnetic interference shielding, *Compos. B Eng.* 190 (2020), 107935.
- [54] N. Zhang, Y. Huang, X. Liu, M. Wang, High efficiency microwave absorption nanocomposites of multiple-phase core-shell CoNi alloy@C loaded on rGO conducting network, *Compos. A Appl. Sci. Manuf.* 115 (2018) 283–293.
- [55] M. Arjmand, A.A. Moud, Y. Li, U. Sundararaj, Outstanding electromagnetic interference shielding of silver nanowires: comparison with carbon nanotubes, *RSC Adv.* 5 (2015) 56590–56598.